Inorg. Chem. **2007**, *46*, 10707–10716

Mechanistic Insights into the Chemistry of Ru(II) Complexes Containing Cl and DMSO Ligands

Joaquim Mola,[†] Isabel Romero,*[,†] Montserrat Rodríguez,[†] Fernando Bozoglian,[‡] Albert Poater,[†,§] Miquel Solà,*[,†] Teodor Parella,[||] Jordi Benet-Buchholz,[‡] Xavier Fontrodona,[†] and Antoni Llobet*[,‡,||]

Departament de Química, Institut de Química Computacional and Servei de RMN, Universitat de Girona, Campus de Montilivi, E-17071 Girona, Spain, Institute of Chemical Research of Catalonia (ICIQ), Av. Països Catalans 16, E-43007 Tarragona, Spain, Dipartimento di Chimica, Università degli Studi di Salerno, via Ponte don Melillo, Fisciano (SA), 84084, Italy, Departament de Química and Servei de RMN, Universitat Autònoma de Barcelona, Cerdanyola del Vallès, E-08193 Barcelona, Spain

Received July 17, 2007

Two new isomers *trans,mer*-[$Ru^{II}Cl_2$(bpea)(DMSO)], **2a**, and *cis,fac*-[$Ru^{II}Cl_2$(bpea)(DMSO)], **2b**, (bpea = *N*,*N*-bis-(2-pyridylmethyl)ethylamine), as well as the bis-DMSO complex *trans,fac*-[$Ru^{II}Cl(bpea)(DMSO)_2$]Cl, **3**, have been synthesized and characterized by cyclic voltammetry and UV-vis and 1D and 2D NMR spectroscopy in solution. Their solid-state structure has also been solved by means of single-crystal X-ray diffraction analysis. All the three complexes display a ruthenium metal center possessing a distorted-octahedral type of coordination, where the bpea ligand is coordinated in a *meridional* fashion in **2a** and in a *facial* fashion in **2b** and **3**. The isomer **2a** is the kinetically favored and thus can be thermally converted into **2b**, that is the thermodynamically favored one. A thorough kinetic analysis strongly points toward a dissociative mechanism, where in the first step a chloro ligand is removed from the metal coordination sphere, followed by a geometric rearrangement before the chloro ligand coordinates again, generating the final complex. DFT calculations agree with the experimental data for the proposed mechanism and allow us to further characterize the mechanism of the **2a** → **2b** rearrangement by obtaining the intermediates and transition state.

Introduction

During the last three decades, the coordination chemistry of ruthenium complexes has experienced a large boost, given the multiple applications they have in the fields of catalysis,[1] photochemistry and photophysics[2] and more recently in supramolecular[3] and bioinorganic[4] chemistry.

To this end, one of the most interesting and promising applications of ruthenium complexes are as chemotherapeutic agents.[5] The majority of the new drugs based on ruthenium complexes that have been prepared and tested lately (some of them already in clinical trials like NAMI-A)[6] are based on coordination complexes of ruthenium that contain chloro, DMSO as well as a pyridylic type of ligands.[7] A major

* To whom correspondence should be addressed. E-mail: marisa.romero@udg.edu (I.R.), miquel.sola@udg.edu (M.S.), allobet@iciq.es (A.L.).

[†] Universitat de Girona.

[‡] Institute of Chemical Research of Catalonia (ICIQ).

[§] Università degli Studi di Salerno.

[||] Universitat Autònoma de Barcelona.

(1) (a) Murahashi, S. I.; Takaya, H.; Naota, T. *Pure Appl. Chem.* **2002**, *74*, 19−24. (b) Naota, T.; Takaya, H.; Murahashi, S. I. *Chem. Rev.* **1998**, *98*, 2599−2660. (c) Rodríguez, M.; Romero, I.; Sens, C.; Llobet, A. *J. Mol. Catal. A: Chem.* **2006**, *251*, 215−220. (d) Rodríguez, M.; Romero, I.; Llobet, A.; Deronzier, A.; Biner, M.; Parella, T.; Stoeckli-Evans, H. *Inorg. Chem*. **2001**, *40*, 4150−4156. (e) Jáuregui-Haza, U. J.; Dessoudeix, M.; Kalck, Ph.; Wilhelm, A. M.; Delmas, H. *Catal. Today*. **2001**, *66*, 297−302.

(2) (a) *Organic and Inorganic Photochemistry*; Ramamurthy, V., Schanze, K. S., Eds.; Marcel Dekker: New York, 1998. (b) Thompson, D. W.; Schoonover, J. R.; Graff, D. K.; Fleming, C. N.; Meyer, T. J. *J. Photochem. Photobiol., A* **2000**, *137*, 131−134. (c) Toma, H. E.; Serrasqueiro, R. M.; Rocha, R. C.; Demets, G. J. F.; Winnischofer, H.; Araki, K.; Ribeiro, P. E. A.; Donnici, C. L. *J. Photochem. Photobiol., A* **2000**, *135*, 185−191. (d) Keefe, M. H.; Benkstein, K. D.; Hupp, J. T. *Coord. Chem. Rev.* **2000**, *205*, 201−228. (e) Romero, M. I.; Rodríguez, M.; Llobet, A.; Collomb-Dunand-Sauthier, M. N.; Deronzier, A.; Parella, T.; Stoeckli-Evans, H. *J. Chem. Soc., Dalton Trans.* **2000**, 1689−1694. (f) Balzani, V.; Juris, A. *Coord. Chem. Rev.* **2001**, *211*, 97−115. (g) Dattelbaum, D. M.; Hartshorn, C. M.; Meyer, T. J. *J. Am. Chem. Soc.* **2002**, *124*, 4938−4939. (h) Nikolau, S.; Toma, H. E. *J. Chem. Soc., Dalton Trans.* **2002**, 352−359. (i) Sala, X.; Romero, I.; Rodríguez, M.; Llobet, A.; González, G.; Martínez, M.; Parella, T.; Benet-Buchholz, J. *Inorg. Chem*. **2004**, *43*, 5403−5409.

10.1021/ic701421w CCC: $37.00
Published on Web 11/15/2007

challenge in this field is to understand the mechanism of action through which those complexes bind to DNA tumor cells. Invariably this process involves π-stacking interactions and/or the substitution of chloro and/or DMSO ligands so that a binding interaction can take place. Thus, it is critical for the advancement of this field to understand the different parameters that govern the substitution chemistry of this type of compounds. Furthermore *cis*- and *trans*-[$RuCl_2(DMSO)_4$] are some of the most widely used starting materials for the synthesis of other ruthenium complexes[8] through the substitution of the labile chloro and DMSO ligands by the desired ligand. The substitution processes are also important to another flourishing area of research that is supramolecular chemistry because Ru−Cl−DMSO complexes are used as building blocks to assemble complex 3D architectures.[9] In the area of catalysis, [$RuCl_2(DMSO)_4$][10] as well as other Ru−Cl−DMSO complexes containing other ligands, are particularly interesting as precursors[11] and catalysts for a variety of reactions including hydrogen-atom transfer,[12] hydrogenation,[13] α-alkylation of ketones,[14] aerobic oxidation of alcohols,[15] oxidation of aliphatic ethers to esters,[16] isomerization of alcohols,[17] selective oxidation of aryl sulfides with molecular oxygen,[18] etc.

With this in mind, we have prepared a family of complexes containing chloro, DMSO, and the tridentate bpea (*N*,*N*-bis-(2-pyridylmethyl)ethylamine) ligand. This ligand is interesting because it generates a very rich chemistry[19] given (a) the different type of coordinating nitrogen atoms (aliphatic vs aromatic) that in turn will generate different trans effects/influences with the consequences this will have to reactivity, (b) the nonequivalence of the three nitrogen atoms that in an octahedral environment will generate different types of geometrical isomers, and (c) the flexibility of the ligand that will allow both a facial and a meridional type of coordination with also the possibility of generating different isomers. This is in sharp contrast with the commonly used trpy (2,2′:6′:2″-terpyridine) ligand that always behaves in a meridional fashion and with all nitrogen-donor atoms being aromatic. All of the mentioned properties of the bpea ligand combined will allow us to extract meaningful information regarding the different parameters that govern the substitution reactions and thus might be useful to interpret/extrapolate Ru−DMSO−Cl interactions with living organisms. Here on, we report the synthesis, isolation, and characterization of a family of Ru−bpea complexes and a detailed analysis of the substitution and isomerization reactions of *trans*,*mer*-[$Ru^{II}(Cl)_2$(bpea)(DMSO)] **2a**.

Experimental Section

Materials. All of the reagents used in the present work were obtained from Aldrich Chemical Co. and were used without further purification. Reagent grade organic solvents were obtained from

(3) (a) Belser, P.; von Zelewsky, A.; Frank, M.; Seel, C.; Vogtle, F.; De Cola, L.; Barigelletti, F.; Balzani, V. *J. Am. Chem. Soc.* **1993**, *115*, 4076−4086. (b) Faiz, J.; Philippopoulos, A. I.; Kontos, A. G.; Falaras, P.; Pikramenou, Z. *Adv. Funct. Mat.* **2007**, *17*, 54−58. (c) Balzani, V.; Bergamini, G.; Marchioni, F.; Ceroni, P. *Coord. Chem. Rev.* **2006**, *250*, 1254−1266.

(4) (a) Kelly, S. O.; Barton, J. K. *Science* **1999**, *238*, 375−381. (b) Hall, D. B.; Holmlin, R. E.; Barton, J. K. *Nature* **1996**, *384*, 731−735. (c) Burrows, C. J.; Muller, J. G. *Chem. Rev.* **1998**, *98*, 1109−1151. (d) Schuster, G. B. *Acc. Chem. Res.* **2000**, *33*, 253−260. (e) Weatherly, S. C.; Yang, I. V.; Thorp, H. H. *J. Am. Chem. Soc.* **2001**, *123*, 1236−1237. (f) Clarke, M. J. *Coord. Chem. Rev*. **2003**, *236*, 209−233. (g) Schmid, W. F.; Zorbas-Seifried, S.; John, R. O.; Arion, V. B.; Jakupec, M. A.; Roller, A.; Galanski, M.; Chiorescu, I.; Zorbas, H.; Keppler, B. K. *Inorg. Chem*. **2007**, *46*, 3645−3656.

(5) Ma, D. L.; Che, C. M.; Siu, F. M.; Yang, M.; Wong, K. W. *Inorg. Chem*. **2007**, *46*, 740−749.

(6) (a) Sava, G.; Alessio, E.; Bergamo, A.; Mestroni, G. Sulfoxide Ruthenium Complexes: Non-Toxic Tools for the Selective Treatment of Solid Tumour Metastases. *Topics in Biological Inorganic Chemistry*; Springer-Verlag GmbH & Co.: Berlin, Germany, 1999; pp 143−169. (b) Sava, G.; Clerici, K.; Capozzi, I.; Cocchietto, M.; Gagliardi, R.; Alessio, E.; Mestroni, G.; Perbellini, A. *Anti-Cancer Drugs* **1999**, *10*, 129−138. (c) Sava, G.; Gagliardi, R.; Bergamo, A.; Alessio, E.; Mestroni, G. *Anticancer Res.* **1999**, *19*, 969−972.

(7) (a) Velders, A. H.; Bergamo, A.; Alessio, E.; Zangrando, E.; Haasnoot, J. G.; Casarsa, C.; Cocchietto, M.; Zorzet, S.; Sava, G. *J. Med. Chem.* **2004**, *47*, 1110−1121. (b) Bratsos, I.; Serli, B.; Zangrando, E.; Katsaros, N.; Alessio, E. *Inorg. Chem*. **2007**, *46*, 975−992.

(8) (a) Evans, I. P.; Spencer, A.; Wilkinson ,J. *J. Chem. Soc., Dalton Trans.* **1973**, *2*, 204−209. (b) Alessio, E.; Mestroni, G.; Nardin, G.; Attia, W. M.; Calligaris, M.; Sava, G.; Zorzet, S. *Inorg. Chem.* **1988**, *27*, 4099−4106. (c) Alessio, E. *Chem. Rev.* **2004**, *104 (9*), 4203−4242.

(9) (a) Ziessel, R.; Grosshenny, V.; Hissler, M.; Stroh, C. *Inorg. Chem.* **2004**, *43*, 4262−4271. (b) Iengo, E.; Zangrando, E.; Minatel, R.; Alessio, E. *J. Am. Chem. Soc*. **2002**, *124*, 1003−1013. (c) Roche, S.; Haslam, C.; Heath, S. L.; Thomas, J. A. *Chem. Commun.* **1998**, *16*, 1681−1682.

(10) a) Tony, K. J. *React. Kinet. Catal. Lett.* **1997**, *60*, 145−155. (b) Kohichi, K. *Organometallics* **1997**, *16*, 2233−2336. (c) Morvillo, A.; Forti, L.; Bressan, M. *New J. Chem.* **1995**, *19*, 951−957.

(11) Okumura, T.; Morishima, Y.; Shiozaki, H.; Yagyu, T.; Funahashi, Y.; Ozawa, T.; Jitsukawa, K.; Masuda, H. *Bull. Chem. Soc. Jpn.* **2007**, *80*, 507−517.

(12) (a) Naz, S.; Adams, H.; Thomas, J. A. *Inorg. Chim. Acta* **2006**, *359*, 759−765. (b) Suresh, I.; Aruna, S. K. *Indian J. Chem., Sect. B: Org. Chem. Incl. Med. Chem.* **2003**, *42B*, 2805−2807. (c) Sens, C.; Rodríguez, M.; Romero, I.; Llobet, A.; Parella, T.; Sullivan, B. P.; Benet-Buchholz, J. *Inorg. Chem*. **2003**, *42*, 2040−2048. (d) Kwong, H. L.; Lee, W. S.; Lai, T. S.; Wong, W. T. *Inorg. Chem. Commun*. **1999**, *2*, 66−69.

(13) Khan, M. M. T.; Mohiuddin, R.; Vancheesan, S.; Swamy, B. *Ind. J. Chem., Sect. A: Inorg. Bioinorg., Phys., Theor. Anal. Chem.* **1981**, *20A*, 564.

(14) Martínez, R.; Brand, G. J.; Ramón, D. J.; Yus, M. *Tetrahedron Lett*. **2005**, *46*, 3683−3686.

(15) Khenkin, A. M.; Shimon, L. J. W.; Neumann, R. *Inorg. Chem*. **2003**, *42*, 3331−3339.

(16) Gonsalvi, L.; Arends, I. W. C. E.; Sheldon, R. A. *Chem. Commun.* **2002**, *3*, 202−203.

(17) van der Drift, R. C.; Sprengers, J. W.; Bouwman, E.; Mul, W. P.; Kooijman, H.; Spek, A. L.; Drent, E. *Eur. J. Inorg. Chem.* **2002**, *8*, 2147−2155.

(18) (a) Srivastava, R. S.; Milani, B.; Alessio, E.; Mestroni, G. *Inorg. Chim. Acta* **1992**, *191*, 15−17. (b) Huynh, M. H. V.; Witham, L. M.; Lasker, J. M.; Wetzler, M.; Mort, B.; Jameson, D. L.; White, P. S.; Takeuchi, K. J. *J. Am. Chem. Soc.* **2003**, *125*, 308−309. (c) Riley, D. P.; Shumate, R. F. *J. Am. Chem. Soc*. **1984**, *106*, 3179−3184.

(19) (a) Rodríguez, M.; Romero, I.; Llobet, A.; Deronzier, A.; Biner, M.; Parella, T.; Stoeckli-Evans, H. *Inorg. Chem.* **2001**, *40*, 4150−4156. (b) Romero, I.; Rodríguez, M.; Llobet, A.; Collomb-Dunand-Sauthier, M. N.; Deronzier, A.; Parella, T.; Stoeckli-Evans, H. *J. Chem. Soc., Dalton Trans.* **2000**, 1689−1694. (c) Romero, I.; Dubois, L.; Collomb-Dunand-Sauthier, M. N.; Deronzier, A.; Latour, J. M.; Pécaut, J. *Inorg. Chem*. **2002**, *41*, 1795−1806. (d) Romero, I.; Collomb-Dunand-Sauthier, M. N.; Deronzier, A.; Llobet, A.; Perret, E.; Pécaut, J.; Le Pape, L.; Latour, J. M. *Eur. J. Inorg. Chem.* **2001**, 64. (e) Dubé, C. E.; Wright, D. W.; Pal, S.; Bonitatebus, P. J.; Armstrong, W. H. *J. Am. Chem. Soc.* **1998**, *120*, 3704−3716. (f) Dubé, C. E.; Mukhopadhyay, S.; Bonitatebus, P. J.; Staples, R. J.; Armstrong, W. H. *Inorg. Chem.* **2005**, *44*, 5161−5175. (g) Mantel, C.; Hassan, A. K.; Pécaut, J.; Deronzier, A.; Collomb-Dunand-Sauthier, M. N.; Duboc-Toia, C. *J. Am. Chem. Soc.* **2002**, *125*, 12337−12344. (h) Pal, S.; Olmstead, M. M.; Armstrong, W. H. *Inorg. Chem.* **1995**, *34*, 4708−4715. (i) Ito, M.; Takita, Y. S.; Sakai, K.; Tubomura, T. *Chem. Lett.* **1998**, 1185−1186.

Chart 1. Drawing of bpea Ligand

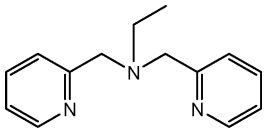

bpea

SDS, and high-purity deionized water was obtained by passing distilled water through a nanopure Mili-Q water purification system. $RuCl_3 \cdot 2H_2O$, was supplied by Johnson and Matthey Ltd. and was used as received.

Preparations. The bpea ligand[20] and complex *fac*-[$RuCl_2$-(DMSO-O)(DMSO-S)$_3$], **1**,[8] (the *fac* here indicates that the tree DMSO sulfur-bonded ligands are bound to the metal center in a facial manner) were prepared according to literature procedures.

All of the synthetic manipulations were routinely performed under a nitrogen atmosphere using Schlenk tubes and vacuum line techniques.

***trans,mer*-[$Ru^{II}Cl_2$(bpea)(DMSO)], 2a.** A solution containing 170 mg (0.74 mmol) of bpea ligand and 360 mg (0.74 mmol) of **1** in 20 mL of dry ethanol was refluxed for 40 min. Upon cooling to room temperature, a dark-orange solid was formed and was filtered on a frit, washed with cold ethanol and ether, and vacuum-dried. Yield: 0.18 g (51%). Anal. Found (Calcd) (%) for $C_{16}H_{23}Cl_2N_3$-ORuS: C 40.16(40.25); N 8.61(8.80); H 4.94(4.85); S 6.90(6.71). IR(cm^{-1}): ν = 3077, 2950, 1446, 1068. ^{1}H NMR (CD_2Cl_2, 500 MHz, 25 °C): δ 8.76 (d, $^3J_{1,14}$−2,13 = 5.25, 2, H_1, H_{14}), 7.63 (t, $^3J_{3-4} = {}^3J_{3-2} = {}^3J_{12-11} = {}^3J_{12-13}$ = 7.62, 2, H_3, H_{12}), 7.27 (d, $^3J_{4,11-3,12}$ = 7.62, 2, H_4, H_{11}), 7.24 (t, 2H, $^3J_{2-1} = {}^3J_{2-3} = {}^3J_{13-12} = {}^3J_{13-14}$ = 7.62, 2, H_2, H_{13}), 5.75 (d, $^2J_{6b,9b-6a,9a}$ = 14.5, 2, H_{6b}, H_{9b}), 4.43 (d, $^2J_{6a,9a-6b,9b}$ = 14.5, 2, H_{6a}, H_{9a}), 3.52 (s, 6, H_{15}, H_{16}), 3.14 (q, 2, $^3J_{7-8}$ = 7.15, H_7), 1.20 (t, $^3J_{8-7}$ = 7.15, 3, H_8). ^{13}C NMR (CD_2Cl_2, 500 MHz, 25 °C):δ 156.7 (C_1, C_{14}), 136 (C_{13}, C_{12}), 124 (C_2, C_{13}), 121.6 (C_4, C_{11}), 61.3 (C_6, C_9), 52 (C_7), 45.5 (C_{15}, C_{16}), 8.5(C_8). NOEs H15 and H16 with H1 and H14; UV−vis (EtOH, 10^{-4}M) λ_{max}, nm (ϵ, $M^{-1}cm^{-1}$): 252 (13 943), 352 (5228), 417 (12 603); $E_{1/2}$ (CH_2Cl_2 + 0.1M TBAP) = 0.53 V versus SSCE (ΔE_p = 190 mV).

***cis,fac*-[$Ru^{II}Cl_2$(bpea)(DMSO)], 2b.** (Cis refers to the position of the DMSO ligand with regard to the aliphatic nitrogen atom of the bpea ligand).

Method 1. This complex was prepared in a manner identical to the case for **2a** except that the reflux was performed for 12 h. An orange solid was obtained. Yield: 0.23 g (63%); Anal. Found (Calcd) (%) for $C_{16}H_{23}Cl_2N_3ORuS$: C 40.20(40.25); N 8.72(8.80); H 4.89(4.85); S 6.84(6.71). IR(cm^{-1}):ν = 3070, 2919, 1481, 1052. ^{1}H NMR (CD_2Cl_2, 500 MHz, 25 °C): δ 9.74 (d, $^3J_{1-2}$ = 5.35, 1, H_1), 9.27 (d, $^3J_{15-13}$ = 5.35, 1, H_{15}), 7.65 (dt, $^3J_{3-2} = {}^3J_{3-4}$ = 7.7, $^4J_{3-1}$ = 1.3, 1, H_3), 7.47 (dt, $^3J_{3-2} = {}^3J_{3-4}$ = 7.7, $^4J_{3-1}$ = 1.3, 1, H_{12}), 7.26 (t, $^3J_{2-1} = {}^3J_{2-3}$ = 7.7, 1, H_2), 7.25 (d, $^3J_{4-3}$ = 7.7, 1, H_4), 7.08 (d, $^3J_{11-12}$ = 7.7, 1, H_{11}), 7.05 (t, $^3J_{13-15} = {}^3J_{13-12}$ = 7.7, 1, H_{13}), 4.52 (d, $^2J_{6a-6b}$ = 15.8, 1, H_{6a}), 4.50 (d, $^2J_{9b-9a}$ = 15.8, 1, H_{9b}), 4.15 (m, $^2J_{7b-7a}$ = 14.5, $^3J_{7b-8}$ = 7.27, 1, H_{7b}), 4.01 (m, $^2J_{7a-7b}$ = 14.5, $^3J_{7a-8}$ = 7.27, 1, H_{7a}), 4.0 (d, $^2J_{9a-9b}$ = 15.8, 1, H_{9a}), 3.92 (d, $^2J_{6b-6a}$ = 15.8, 1, H_{6b}), 3.51 (s, 3, H_{16}), 3.05 (s, 3, H_{17}), 1.29 (t, $^3J_{8-7}$ = 7.27, 3, H_8). ^{13}C NMR (CD_2Cl_2, 500 MHz, 25 °C): δ 154.0 (C_{15}), 152.0 (C_1), 136 (C_3), 134.5 (C_{12}), 123.2 (C_{13}), 122.8 (C_2), 120.4 (C_4), 120.1 (C_{11}), 68.4 (C_9), 67.5 (C_6), 59.6 (C_7), 44.7 (C_{16}), 44.1 (C_{17}), 7.8 (C_8). NOEs H17 with H15 and H16 with H7; UV−vis (EtOH, 10^{-4}M) λ_{max}, nm (ϵ, $M^{-1}cm^{-1}$): 250 (11 787), 327 (6250), 363 (9126); $E_{1/2}$ (CH_2Cl_2 + 0.1M TBAP) = 0.56 V versus SSCE (ΔE_p = 220 mV).

Method 2. This isomer was also obtained from a solution of **2a** in EtOH at 75 °C after 5 h of heating.

***trans,fac*-[$Ru^{II}Cl$(bpea)$(DMSO)_2$]Cl, 3.** (Trans refers to the position of the chloro ligand with regard to the aliphatic-N atom of bpea). A solution containing 0.375 mL (4.34 mmol) of DMSO and 57 mg (0.12 mmol) of *trans,mer*-[$Ru^{II}Cl_2$(bpea)(DMSO)], **2a**, in 30 mL of 1-propanol was heated for 1 h 30 min at 85 °C. After the addition of 10 mL of ether, a yellow solid was formed and filtered on a frit, washed with ether, and vacuum-dried. Yield: 0.045 g (68%). IR (cm^{-1}): ν = 3002, 2921, 1081,1018. ^{1}H NMR (MeOD, 200 MHz, 25 °C): δ 9.40 (d, $^3J_{1,14-2,13}$ = 5.8, 2, H_1, H_{14}), 8.06 (t, $^3J_{3-4} = {}^3J_{3-2} = {}^3J_{12-11} = {}^3J_{12-13}$ = 7.8, 2, H_3, H_{12}), 7.7 (d, $^3J_{4,11-3,12}$ = 7.8, 2, H_4, H_{11}), 7.57 (t, $^3J_{2-1} = {}^3J_{2-3} = {}^3J_{13-12} = {}^3J_{13-14}$ = 7.8, 2, H_2, H_{13}), 5.01 (d, $^2J_{6a,9a-6b,9b}$ = 16.8, 2, H_{6a}, H_{9a}), 4.73 (d, $^2J_{6b,9b-6a,9a}$ = 16.8, 2, H_{6b}, H_{9b}), 4.12 (q, $^3J_7$−8 = 7.4, 2, H_7), 3.65 (s, 6, H_{15}, H_{18}), 3.03 (s, 6, H_{16}, H_{17}), 1.59 (t, $^3J_8$−7 = 7.4, 3, H_8). ^{13}C NMR (MeOD, 200 MHz, 25 °C):δ 163.1 (C_5, C_{10}), 151.9 (C_1, C_{14}), 140.6 (C_3, C_{12}), 126.1 (C_4, C_{11}), 123.7 (C_2, C_{13}), 69.3 (C_6, C_9), 64.1 (C_7), 47.6 (C_{15}, C_{18}), 46.2 (C_{16}, C_{17}), 8.81 (C_8). UV−vis (EtOH, 10^{-4}M) λ_{max}, nm (ϵ, $M^{-1}cm^{-1}$): 240 (14 542), 275 (11 034), 293(sh); $E_{1/2}$ (CH_2Cl_2 + 0.1M TBAP) = 1.04 V versus SSCE (ΔE_p = 260 mV).

Instrumentation and Measurements. FTIR spectra were taken in a Mattson-Galaxy Satellite FTIR spectrophotometer containing an MKII Golden Gate Single Reflection ATR System. UV−vis spectroscopy was performed on a Cary 50 Scan (Varian) UV−vis spectrophotometer with 1 cm quartz cells or with an immersion probe of 5 mm path length. Cyclic voltammetric experiments were performed in an IJ-Cambria IH-660 potentiostat using a three-electrode cell. A glassy carbon-disk electrode (3 mm diameter) was used as working electrode, platinum wire as auxiliary, and SSCE as the reference electrode. All of the cyclic voltammograms presented in this work were recorded under a nitrogen atmosphere unless explicitly mentioned. The complexes were dissolved in previously degassed solvents containing the necessary amount of *n*-$Bu_4N^+PF_6^-$ (TBAH) as a supporting electrolyte, to yield a 0.1 M ionic strength solution. All of the $E_{1/2}$ values reported in this work were estimated from cyclic voltammetric experiments as the average of the oxidative and reductive peak potentials ($E_{p,a} + E_{p,c}$)/2. Unless explicitly mentioned, the concentration of the complexes was approximately 1 mM. The ^{1}H NMR spectroscopy was performed on a Bruker DPX 200 MHz or a Bruker 500 MHz. Samples were run in CD_2Cl_2 with internal references (residual protons and/or tetramethylsilane) and also in MeOD. Elemental analyses were performed using a CHNS−O Elemental Analyzer EA-1108 from Fisons.

Kinetics. The reactions were followed by UV−vis spectroscopy in the 600−330 nm range where none of the solvents absorbs. Two spectrophotometers were used, a JM TIDAS II with a 661.202-UVS immersion probe and a PolyScience thermostatic bath, or a Shimadzu UV-2401PC with a peltier accessory. In all cases, the temperature was maintained at ±0.1 °C. Observed rate constants were derived from absorbance versus time traces at the wavelengths where a maximum increase and/or decrease of absorbance were observed or by a global fitting method. Table S2 in the Supporting Information collects all of the obtained k_{obs} values as a function of chloride concentration, solvent, and temperature. Traces were fitted to two exponential first-order consecutive reactions. In all of the cases, the chloride concentration was at least 10 times higher than

(20) Pal, S.; Chan, M. K.; Armstrong, W. H. *J. Am. Chem. Soc.* **1992**, *114*, 6398−6406.

Table 1. Crystal Data for X-ray Structures of **2a**, **2b**, and **3**

	2a	**2b**	**3**
empirical formula	$C_{16}H_{23}Cl_2N_3ORuS$	$C_{16}H_{23}Cl_2N_3ORuS$	$C_{20}H_{37}Cl_2N_3O_4RuS_2$
fw	477.40	477.40	619.62
cryst syst	monoclinic	monoclinic	monoclinic
space group	*P*21/*c*	*P*2(1)/*n*	*P*1 21/*n* 1
a (Å)	9.4262(17)	9.9997(2)	9.503(4)
b (Å)	26.571(15)	13.3928(3)	11.590(5)
c (Å)	7.8177(15)	13.9841(3)	23.607(9)
α (deg)	90	90	90
β (deg)	112.251(3)	91.5940(10)	91.805(7)
γ (deg)	90	90	90
V (Å^3)	1812.3(6)	1872.08(7)	2598.8(18)
formula units/cell	4	4	4
ρ_{calcd} (g•cm^{-3})	1.750	1.694	1.715
μ (mm^{-1})	1.284	1.243	1.584
GOF on F^2	1.175	1.042	1.009
$R1^a$, $[I > 2\sigma(I)]$	0.0420	0.0301	0.0350
$wR2^b$ (all data)	0.1083	0.0788	0.0819

[a] $R1 = \sum||F_o| - |F_c||/\sum|F_o|$. [b] $wR2 = [\sum\{w(F_o^2 - F_c^2)^2\}/\sum\{w(F_o^2)^2\}]^{1/2}$, where $w = 1/[\sigma^2(F_o^2) + (0.0042P)^2]$ and $P = (F_o^2 + 2F_c^2)/3$.

the ruthenium complex concentration, which was maintained in the range $(0.2-6.0) \times 10^{-4}$ M. Ionic strength was maintained constant at 1 M $LiClO_4$. All of the fittings were carried out with the *Specfit* program from Spectrum Software Associates.

X-ray Structure Determination. Suitable crystals of **2a** were grown from acetone as orange blocks. Suitable crystals of **2b** and **3** were grown by slow diffusion of ethyl ether into a MeOH solution of the compound as orange blocks and light-yellow plates, respectively. Measurement of the crystals was performed on a Bruker Smart Apex CCD diffractometer using graphite-monochromated Mo Kα radiation ($\lambda = 0.71073$ Å) from an X-ray tube. Data collection, *SMART* version 5.631 (BrukerAXS 1997−02); data reduction, *Saint+* version 6.36A (Bruker AXS 2001); absorption correction, *SADABS* version 2.10 (Bruker AXS 2001) and structure solution and refinement, *SHELXTL* version 6.14 (Bruker AXS 2000−2003). The crystallographic data as well as details of the structure solution and refinement procedures are reported in Table 1. CCDC 650406, 650407, and 650408 contain the supplementary crystallographic data for this article. These data can be obtained free of charge from the Cambridge Crystallographic Data Centre via www.ccdc.cam.ac.uk/data_request/cif.

Computational Details. The density functional theory (DFT) calculations have been carried out with the hybrid B3PW91 density functional,[21,22] as implemented in the *Gaussian 03* package.[23] The ruthenium atoms have been represented with the quasi-relativistic effective core pseudo-potentials of the Stuttgart group and the associated basis sets augmented with a polarization function ($\alpha = 1.235$).[24,25] The remaining atoms (carbon, oxygen, and hydrogen) have been represented with 6-31++G(d,p) basis sets.[26] The B3PW91 geometry optimizations were performed without any symmetry constraints, and the nature of the extrema (local minima or transition states) was checked by analytical frequency calculations. The energies given throughout the article are electronic energies with the ZPE corrections (however, inclusion of the ZPE corrections does not significantly modify the results) or Gibbs free energy values at 298 or 353 K and $P = 1$ atm. The atomic charges have been calculated using the natural population analysis scheme of Weinhold and co-workers.[27] The solvent effect was introduced by the polarizable continuum model (PCM), implemented by Tomasi and co-workers.[28] The cavity is created via a series of overlapping spheres.

The optimization of **2a** in the gas phase agrees with the experimental X-ray data. The standard deviation for the bond distances and angles given in Table S1 in the Supporting Information are only 0.014 Å and 0.8°,[29] respectively, thus providing confidence in the reliability of the chosen method to reproduce geometries of the studied complexes. For **2b**, only minor differences in the C−C−N and C−N−C angles of the bpea ligand are found. Nevertheless, these small differences can be attributed to packing effects. The calculated structure for **3** also nicely reproduces the experimental structure obtained from X-ray data. XYZ coordinates of the calculated structures for **2a**, **2b**, and **3**, and for all of the other calculated complexes (intermediates and transition states) are presented in the Supporting Information section.

Results and Discussion

Synthesis and Structure. The reaction of equimolecular amounts of *fac*-[$RuCl_2$(DMSO-O)(DMSO-S)$_3$], **1**, and bpea in ethanol at reflux for 40 min produces the kinetically favored *trans,mer*-[$Ru^{II}Cl_2$(bpea)(DMSO)], **2a**, complex in moderate yield. Additional reflux to 12 h generates the thermodynamically favored *cis,fac*-[$Ru^{II}Cl_2$(bpea)(DMSO)], **2b**, isomer as shown in Scheme 1. In octahedral complexes, the bpea ligand can potentially adopt a facial or meridional

(21) Becke, A. D. *J. Chem. Phys*. **1993**, *98*, 5648−5652.
(22) Perdew, J. P.; Wang, Y. *Phys. Rev. B* **1992**, *45*, 13244−13249.
(23) Frisch, M. J.; Trucks, G. W.; Schlegel, H. B.; Scuseria, G. E.; Robb, M. A.; Cheeseman, J. R.; Montgomery, J. A., Jr.; Vreven, T.; Kudin, K. N.; Burant, J. C.; Millam, J. M.; Iyengar, S. S.; Tomasi, J.; Barone, V.; Mennucci, B.; Cossi, M.; Scalmani, G.; Rega, N.; Petersson, G. A.; Nakatsuji, H.; Hada, M.; Ehara, M.; Toyota, K.; Fukuda, R.; Hasegawa, J.; Ishida, M.; Nakajima, T.; Honda, Y.; Kitao, O.; Nakai, H.; Klene, M.; Li, X.; Knox, J. E.; Hratchian, H. P.; Cross, J. B.; Bakken, V.; Adamo, C.; Jaramillo, J.; Gomperts, R.; Stratmann, R. E.; Yazyev, O.; Austin, A. J.; Cammi, R.; Pomelli, C.; Ochterski, J. W.; Ayala, P. Y.; Morokuma, K.; Voth, G. A.; Salvador, P.; Dannenberg, J. J.; Zakrzewski, V. G.; Dapprich, S.; Daniels, A. D.; Strain, M. C.; Farkas, O.; Malick, D. K.; Rabuck, A. D.; Raghavachari, K.; Foresman, J. B.; Ortiz, J. V.; Cui, Q.; Baboul, A. G.; Clifford, S.; Cioslowski, J.; Stefanov, B. B.; Liu, G.; Liashenko, A.; Piskorz, P.; Komaromi, I.; Martin, R. L.; Fox, D. J.; Keith, T.; Al-Laham, M. A.; Peng, C. Y.; Nanayakkara, A.; Challacombe, M.; Gill, P. M. W.; Johnson, B.; Chen, W.; Wong, M. W.; Gonzalez, C.; Pople, J. A. *Gaussian 03*, revision C.02; Gaussian, Inc.: Wallingford, CT, 2004.
(24) Andrae, D.; Haussermann, U.; Dolg, M.; Stoll, H.; Preuss, H. *Theor. Chim. Acta* **1990**, *77*, 123−141.
(25) Bergner, A.; Dolg, M.; Kuchle, W.; Stoll, H.; Preuss, H. *Mol. Phys.* **1993**, *80*, 1431−1444.
(26) Hehre, W. J.; Ditchfield, R.; Pople, J. A. *J. Chem. Phys*. **1972**, *56*, 2257−2261.
(27) Reed, A. E.; Curtiss, L. A.; Weinhold, F. *Chem. Rev*. **1988**, *88*, 899−926.
(28) Barone, V.; Cossi, M. *J. Phys. Chem. A* **1998**, *102*, 1995−2001.
(29) Standard deviations for the distances and for the angles, $s_{n-1} = \sqrt{\sum_{i=1}^{N}(CV - EV)^2/(N-1)}$, where *CV* means calculated value, *EV* experimental value (X-ray data), and *N* is the number of distances or angles taken into account.
(30) (a) Laurent, F.; Plantalech, E.; Donnadieu, B.; Jiménez, A.; Hernández, F.; Martínez-Ripoll, M.; Biner, M.; Llobet, A. *Polyhedron* **1999**, *18*, 3321−3331. (b) Sens, C.; Rodríguez, M.; Romero, I.; Llobet, A.; Parella, T.; Sullivan, B. P.; Benet-Buchholz, J. *Inorg. Chem*. **2003**, *42*, 2040−2048. (c) Sens, C.; Rodríguez, M.; Romero, I.; Llobet, A.; Parella, T.; Benet-Buchholz, J. *Inorg. Chem.* **2003**, *42*, 8385−8394. (d) Sala, X.; Poater, A.; Romero, I.; Rodríguez, M.; Llobet, A.; Solans, X.; Parella, T.; Santos, T. M. *Eur. J. Inorg. Chem.* **2004**, 612−618. (e) Katz, N. E.; Romero, I.; Llobet, A.; Parella, T.; Benet-Buchholz, J. *Eur. J. Inorg. Chem*. **2005**, 272−277. (f) Katz, N. E.; Fagalde, F.; Katz, N. D. L.; Mellace, M. G.; Romero, I.; Llobet, A.; Benet-Buchholz, J. *Eur. J. Inorg. Chem*. **2005**, 3019−3023. (g) Serrano, I.; Llobet, A.; Rodríguez, M.; Romero, I.; Benet-Buchholz, J.; Parella, T.; Campelo, J.; Luna, D.; Marinas, J. *Inorg. Chem*. **2006**, *45* (6),

Scheme 1

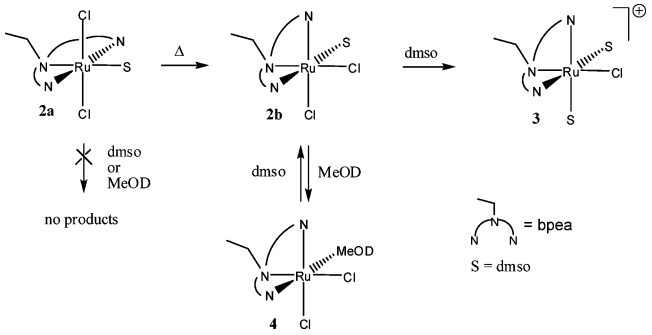

coordination mode because of its flexibility.[19] The former mode is the most usually found in the literature and agrees with the fact that **2b** is the thermodynamically favored isomer. On the other hand, the trans,mer isomer **2a** is the first crystallographically characterized ruthenium complex with the bpea ligand acting in a meridional manner. The reaction of **2a** with excess DMSO generates the bis-DMSO complex *trans,fac*-[Ru^{II}Cl(bpea)$(DMSO)_2$]Cl, **3**, that is formed through **2b** (Scheme 1), as will be shown in the kinetic section below.

Crystallographic data and selected structural parameters for **2a**, **2b**, and **3** are presented in Tables 1 and 2 respectively and in the Supporting Information section together with the CIF files. An *ORTEP* plot for **2a**, **2b**, and for the cationic moiety of **3** is presented in Figure 1 with the corresponding atomic labels.

2a, **2b**, and **3** present a distorted-octahedral type of geometry around the metal center, as expected for low spin d^6 ruthenium ion. Bond distances and angles are within the values observed for this type of complexes.[30] The Ru−S bond for **3** is 35−40 pm larger than those for **2a** and **2b**, a phenomenon associated with steric repulsion between DMSO ligands situated in a cis manner in octahedral geometries.[8b] The DMSO ligands in the three complexes also present weak-to-medium intramolecular hydrogen bonds with bpea (the associated metric parameters are as follows: **2a**, C14−H14a−O1 (C14−H14a, 0.950 Å; H14a−O1, 2.534 Å; C14−O1, 3.145 Å; 139.59°); **2b**, C7−H7b−O1 (0.991 Å, 2.188 Å, 3.063 Å, 146.44°); **3**, C15−H15b−O2 (0.960 Å, 2.546 Å, 3.278 Å, 133.07°), C7−H7a−O2 (0.970 Å, 2.590 Å, 3.188 Å, 120.05°), C7−H7b−O1 (0.969 Å, 2.279 Å, 3.122 Å, 144.93°), C6−H6a−O1 (0.970 Å, 2.500 Å, 3.240 Å, 132.97°)).

Spectroscopic and Redox Properties. IR spectra for **2a** and **2b** are relatively similar, with a band at 1052 and 1068 cm^{-1}, respectively, that can be assigned to a ν_{so} stretching (Figure S4 in the Supporting Information). The absence of any significant vibration in the 920−930 cm^{-1} range indicates a sulfur-bonded DMSO complex.[31,32]

1D and 2D NMR spectra of **2a**, **2b**, and **3** are presented in the Supporting Information section. All of the resonances can be unambiguously assigned taking into consideration the symmetry of the individual complexes and are fully consistent with the structure presented in the solid state. All of the labels used with the NMR data are keyed with regard to the labels used in the crystal structures of **2a**, **2b**, and **3** (Figure 1). It is worth mentioning here that the methylenic resonances of the N−CH_2−py group of the bpea ligand can be used as a diagnosis for the facial or meridional coordination. In the latter case, the resonances of H6b and H9b for **2a** appear close to 6 ppm and are more than 1 ppm downfield with regard to the facial case. This phenomenon had been previously observed for related bpea−phosphine complexes.[33] The coordination mode of bpea also shifts the resonances of the methylenic H7 protons, changing from 3.14 ppm in the *trans,mer*-**2a** isomer to 4.09 and 4.15 in the facial **2b**, due to the different location of these protons with regard to the aromatic ring current of the bpea pyridyl groups. Both methylenic H7a−b protons are diastereotopic in the *cis,fac*-**2b** complex due to the asymmetry of the molecule.

Another interesting feature of the NMR spectra is the intraligand NOEs observed between DMSO and bpea. For the case of **2a**, a NOE signal is observed between the methyl groups of the DMSO ligand (C15, C16) and both aromatic H1a and H14a, which are found to be magnetically equivalent, thus indicating that the intramolecular hydrogen bond H14a−O1 found in the solid state is lost in solution and that the DMSO ligand is rotating through the Ru−S bond.

The electronic spectra of **2a**, **2b**, and **3** are shown in Figure 2 and in the Supporting Information (Figure S5). The complexes present ligand-based $\pi-\pi^*$ transitions below 300 nm and above 300 nm bands that can be assigned to a series of MLCT, $d\pi-\pi^*$(Ru−bpea);[19a] A bathochromic shift is observed for the trans complex versus the cis (λ_{max} = 417 nm (ϵ = 12 603) and 352 nm (ϵ = 5228) for **2a**, 363 nm (ϵ = 9126) and 327 nm (ϵ = 6250) for **2b**). The same behavior has been recently observed for related Ru−terpyridine complexes[9a] and can be interpreted in terms of crystal field theory. For **2b**, the cis arrangement of the chloro ligands allows the exertion of a trans influence over the N−bpea atoms that produce a stronger crystal-field splitting. This generates a HOMO orbital lower in energy, whereas the π^*-based LUMO remains virtually unchanged. This is also in agreement with the redox potentials obtained in the cyclic voltammogram (Supporting Information) for the Ru(III/II) couple that is anodically shifted by 30 mV for the *cis,fac*-**2b** isomer with regard to the *trans,mer*-**2a** and also with the higher thermodynamic stability obtained for **2b** over **2a** by DFT calculations (vide infra).

Kinetics. Thermal isomerization kinetics of **2a** to **2b** and of their ligand substitution reactions were thoroughly studied at different temperatures, solvents, and concentration of **2a**,

2644−2651. (h) Masllorens, E.; Rodríguez, M.; Romero, I.; Roglans, A.; Parella, T.; Benet-Buchholz, J.; Poyatos, M.; Llobet, A. *J. Am. Chem. Soc.* **2006**, *128*, 5306−5307. (i) Sala, X.; Rodríguez, A. M.; Rodríguez, M.; Romero, I.; Llobet, A.; von Zelewsky, A.; Benet-Buchholz, J. *J. Org. Chem.* **2006**, *71*, 9283−9290.

(31) Smith, M. K.; Gibson, J. A.; Young, C. G.; Broomhead, J. A.; Junk, P. C.; Keene, F. R. *Eur. J. Inorg. Chem.* **2000**, 1365−1370.
(32) Calligaris, M.; Carugo, O. *Coord. Chem. Rev.* **1996**, *15*, 83−154.
(33) Mola, J.; Romero, I.; Rodríguez, M.; Llobet, A.; Parella, T.; Benet-Buchholz, J.; Poater, A.; Duran, M.; Solà, M. *Inorg. Chem.* **2006**, *45*, 10520−10529.

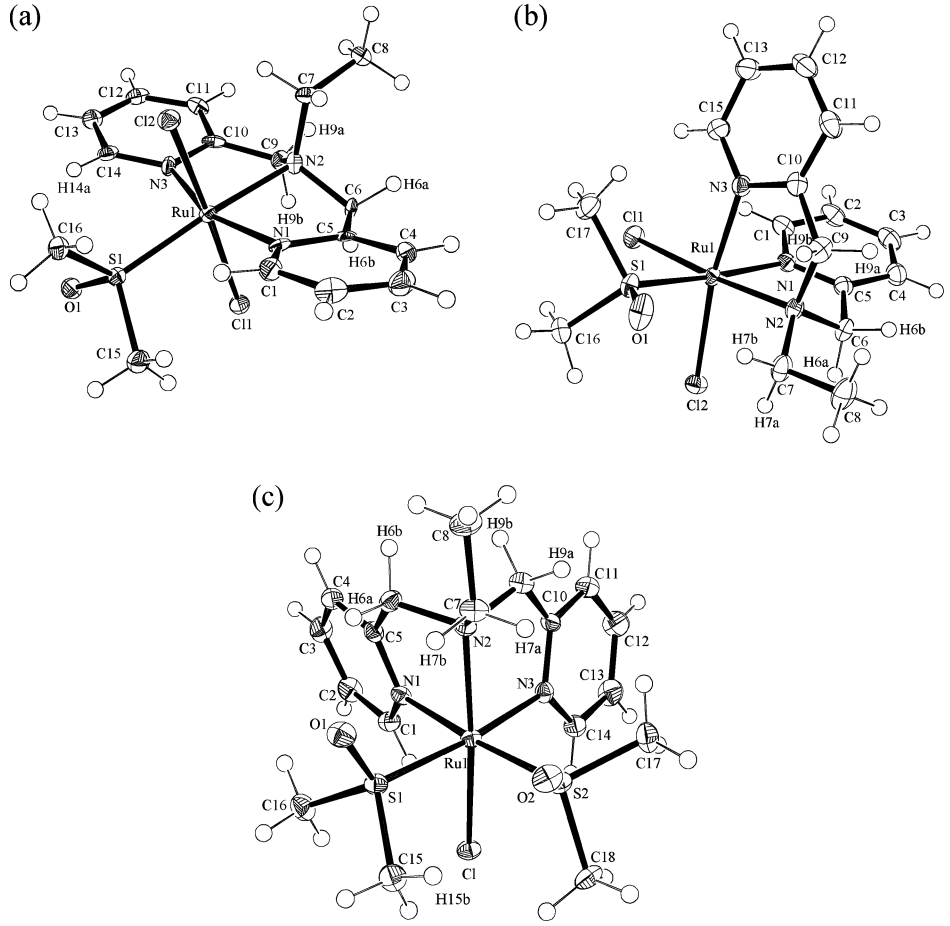

Figure 1. X-ray structures (Ortep plots with ellipsoids at the 50% probability level) and a labeling scheme for (a) **2a**, (b) **2b**, (c) and **3**.

Cl^-, and DMSO, by UV−vis repetitive scans using *SPECFIT* to fit the data and extract kinetic and thermodynamic parameters.

Part a of Figure 2 shows the spectral changes every 10 min that occur when a 2×10^{-4} M solution of **2a** with a 100-fold excess of DMSO (no Cl^- added to the system) in methanol is maintained at 50.0 °C. Mathematical treatment of the data shows the presence of two consecutive reactions: initially the isomerization of **2a** to **2b** (with an estimated $k_{iso} = 0.018$ min^{-1}) and then the substitution of one chloro ligand of **2b** by DMSO to generate the bis-DMSO complex **3** ($k_{subst} = 0.029$ min^{-1}). **3** was also prepared as shown in Scheme 1 and in the Experimental Section and was spectroscopically characterized. The mathematical treatment of the above repetitive scans allows us also to obtain the calculated spectra shown in part b of Figure 2 that are in very good agreement with the experimental spectra of authentic samples (Figure S5 in the Supporting Information).

To elucidate the isomerization reaction mechanism, a series of experiments were performed in methanol at different [Cl^-] (from 2×10^{-4} to 8×10^{-3} M) and temperatures (from 30 to 60 °C), with no DMSO added to the system. Repetitive-scan spectra show initially a clear isosbestic point at 394 nm. When long reaction times were required, the isosbestic point was lost, and an increase followed by a decrease in absorbance at 385 nm was observed. The kinetic traces can be fitted to a model involving two consecutive first-order reactions. The first reaction corresponds to the isomerization of **2a** to **2b**, according to the UV−vis and ^{1}H NMR spectra, with a rate constant that shows an inverse dependence with the [Cl^-] (part a of Figure 3). The second reaction step is independent of [Cl^-]. The calculated pseudo-first-order constants of both reactions are summarized in Table S2 in the Supporting Information. To investigate the second reaction, experiments were performed with **2a** in CD_3OD and studied by ^{1}H and ^{13}C NMR. The NMR signals showed the first isomerization reaction from **2a** to **2b** already mentioned, and a second reaction where the ^{1}H NMR signals of coordinated DMSO disappear and a signal corresponding to free DMSO appears. After completion of the reaction, ^{13}C NMR shows only free DMSO and a heptuplete corresponding to coordinated CD_3OD. On the basis of this data, the species *cis*,*fac*-[$RuCl_2$(bpea)(CD_3OD)] is proposed as the final product (Scheme 1 and Figure S8 in the Supporting Information). Kinetic constants for this experiment were calculated using integrals from peaks corresponding to aromatic protons for the reaction from **2a** to **2b** and the disappearance of coordinated DMSO for reaction from **2b** to **4**. The values obtained for the rate constants agree (±10%) with the ones calculated by UV−vis measurements.

It is important to note here that when this experiment was performed with **2a** at [Cl^-] = 0.1 M, neither isomerization nor substitution were observed in the same time scale,

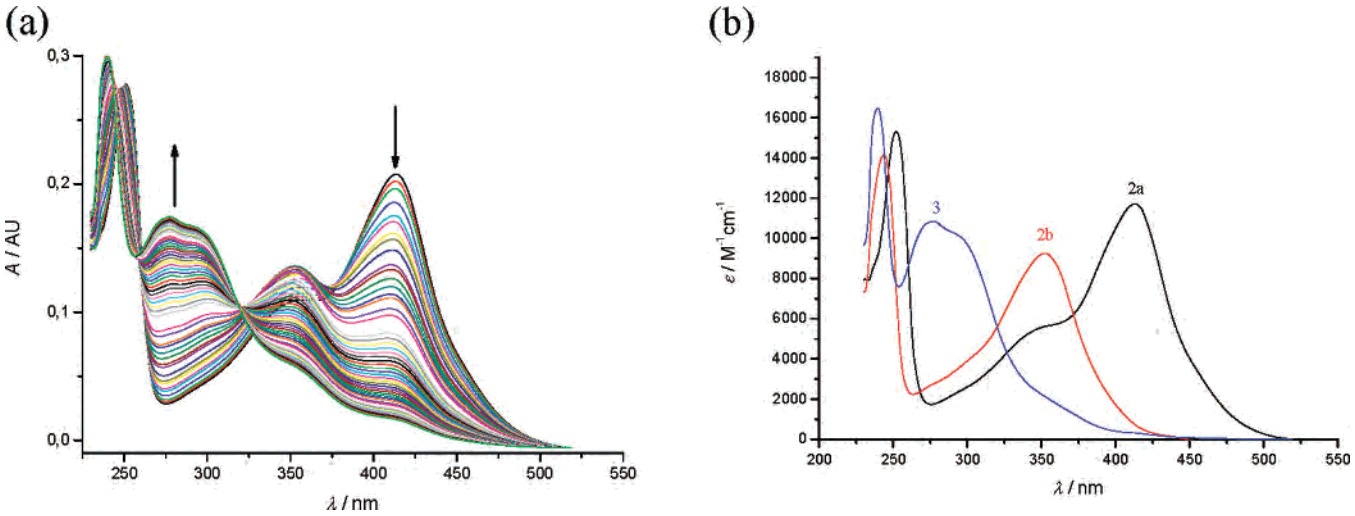

Figure 2. (a) UV−vis spectral changes obtained at 50 °C for the isomerization of **2a** into **2b** in the presence of excess DMSO ([2a] = 1×10^{-4} M; [DMSO] = 0.01 M) measured every 2 min for 4 h. (b) Calculated spectra for the species involved using *SPECFIT*.

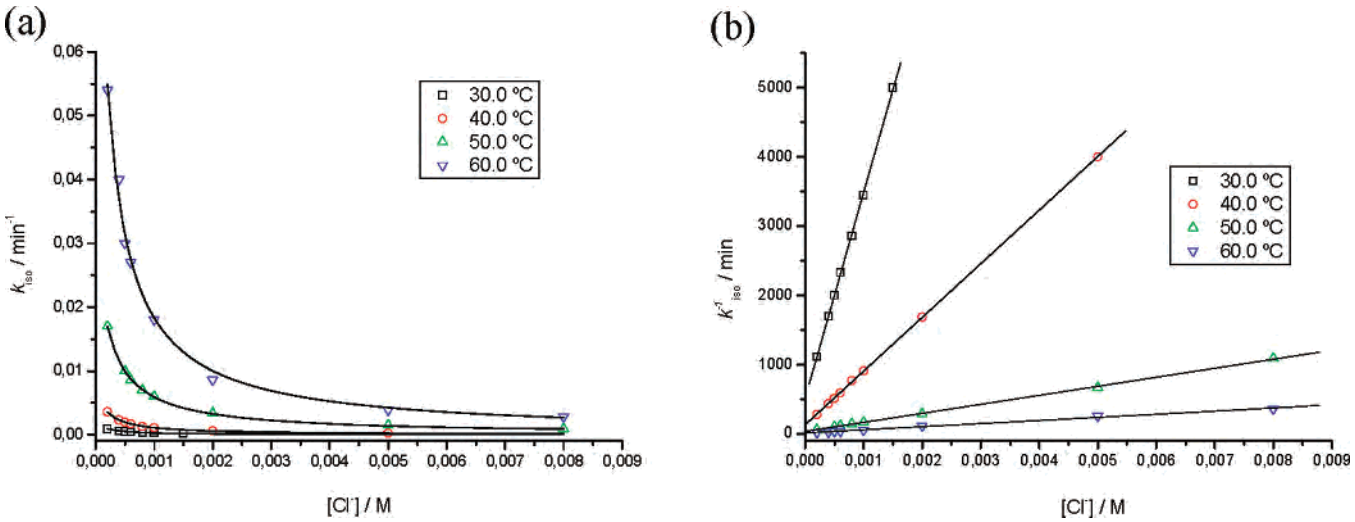

Figure 3. (a) Plot of the first-order rate constant k_{iso} versus [Cl$^-$] for the isomerization reaction from **2a** to **2b** in methanol ([2a] = 2×10^{-4} M). (b) Plot of $1/k_{iso}$ versus [Cl$^-$] for the isomerization from **2a** to **2b** in methanol ([2a] = 2×10^{-4} M).

Table 2. Selected Bond Lengths (Angstroms) for **2a**, **2b**, and **3**

	2a	**2b**	**3**
Ru1−N3	2.070(4)	2.0420(13)	2.094(2)
Ru1−N1	2.085(4)	2.1028(13)	2.101(2)
Ru1−N2	2.153(4)	2.1354 (13)	2.143(2)
Ru1−S1	2.2236(13)	2.2412(5)	2.2776(9)
Ru1−Cl2	2.4117(13)	2.4249(4)	2.2642(9)[a]
Ru1−Cl1	2.4378(13)	2.4414(4)	2.4110(1)

[a] Ru−S2 bond length.

Table 3. First-Order Rate Constants for the Isomerization of **2a** to **2b** Measured at 60 °C

entry	solvent	relative polarity[34]	acceptor number[35]	**[2a]** (mM)	[Cl$^-$] (mM)	$k_{obs} \times 10^2$ (min^{-1})
1				0.05	0.5	3.1
2				0.10	0.5	2.9
3	methanol	0.762	4.13	0.20	0.5	2.8
4				0.60	0.5	3.2
5				0.05	0.05	5.4
6	ethanol	0.654	3.71	0.05	0.05	2.7
7	1-propanol	0.617	3.77	0.05	0.05	1.8
8	2-propanol	0.564	3.37	0.05	0.05	1.1

proving that this substitution reaction only takes place once the cis isomer is formed.

Two more observations are crucial to reinforce the proposed reaction mechanism: (a) the isomerization reaction is first order with respect to complex concentration, as can be seen from data in Table 3 (entry 1−4), and (b) Table 3 (entry 5−8) shows that an increase in solvent polarity[34] and acceptor number[35] results in an increase in reaction rates, suggesting that the isomerization reaction takes place through an intermediate or a transition state that presents a charge distribution stabilized by polar solvents.

In part a of Figure 3 the plots of k_{iso} versus [Cl$^-$] at different temperatures show an inverse dependence of the reaction rate with chloride concentration. This dependence is indicative of a pre-equilibrium, where one chloro ligand dissociates prior to the isomerization process itself. This fact supports a dissociative mechanism rather than an intramolecular one. On the basis of all of the information mentioned

(34) Reichardt, C. *Solvents and Solvent Effects in Organic Chemistry*, 2nd ed.; VCH Publishers: New York, 1988.
(35) Gutmann, V.; Resch, G.; Linert, W. *Coord. Chem. Rev.* **1982**, *43*, 133.

Scheme 2

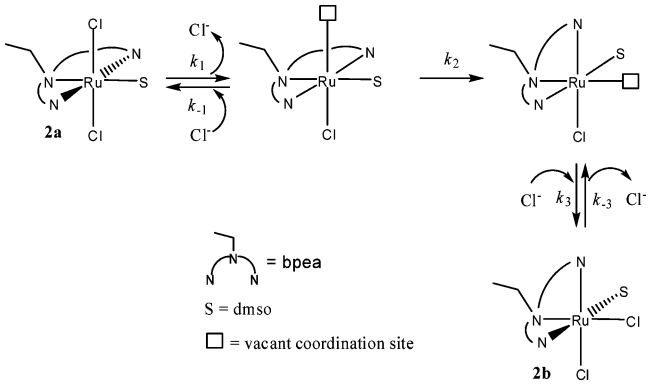

above and considering similar systems already reported in the literature,[36] the reaction mechanism shown in Scheme 2 is proposed. The first step corresponds to the dissociation of one chloro ligand to generate a pentacoordinated species. The second step involves the rearrangement of the bpea ligand to achieve the final *fac* configuration. In the final step, the chloride anion enters trans to the aliphatic nitrogen of the bpea ligand to generate the final *cis,fac* product. Although the first step and this final step are dissociation equilibria, the electronic environment of the chloro ligand is very different. Whereas in the first case the two chloro ligands are trans to one another, in the final step, the chloride anion enters trans to an aliphatic nitrogen with a larger trans effect that strongly influences reaction rates, making this final reaction step faster than the first one.[37]

Using the stationary state approximation, the rate law derived from the proposed mechanism corresponds to the following equation,

$$v = \frac{k_1 k_2}{k_{-1}[\mathrm{Cl}^-] + k_2}\,[\textit{trans,mer}\text{-}[\mathrm{RuCl_2(DMSO)(bpea)}]] \quad (1)$$

And in excess of chloride (pseudo first-order conditions), the observed rate constant k_{iso} can be expressed as shown in eq 2 and 3.

$$k_{iso} = \frac{k_1 k_2}{k_{-1}[\mathrm{Cl}^-] + k_2} \quad (2)$$

$$\frac{1}{k_{iso}} = \frac{k_{-1}[\mathrm{Cl}^-]}{k_1 k_2} + \frac{1}{k_1} \quad (3)$$

From the plots of $1/k_{iso}$ versus $[Cl^-]$, the values of k_1 and K_1k_2 ($K_1 = k_1/k_{-1}$) can be determined (part b of Figure 3). A value of $K_1k_2 = 5.9 \times 10^{-9}$ M·min^{-1} is obtained directly from the slope of the plot of eq 2. Their associated thermal activation parameters are obtained from the corresponding Eyring plots (Supporting Information) and are $\Delta H^{\ddagger} = 32 \pm 1$ kcal·mol^{-1} and $\Delta S^{\ddagger} = 13.4$ cal·mol^{-1}·K^{-1}. The high value obtained for $\Delta H^{\ddagger}$ reflects the need for bond breaking to generate the pentacoordinated species and the subsequent rearrangement from mer to fac. With regard to $\Delta S^{\ddagger}$, considering that $\Delta S°$ for K_1 is expected to be positive because charged species are generated, activation entropy for the second step of the mechanism, $\Delta S^{\ddagger}$ (k_2), has to be close to zero, in agreement with the proposed mechanism where the second step involves only a rearrangement with a low entropic barrier. All of the experiments and activation parameters support the dissociative mechanism proposed with a pentacoordinated transition state.

Computational Results. To get further insight into stability of the involved species, the electronic and structural nature of initial complexes, the products, the reaction intermediates, and the transition states involved in the **2a** → **2b** rearrangement, we have carried out a theoretical analysis based on DFT calculations.

The computation of **2a** and **2b** shows that **2a** is 5.2 kcal·mol^{-1} less stable than **2b** in the gas phase, and this gap grows to 7.1 kcal·mol^{-1} in solution, using the PCM solvent method for ethanol. The Gibbs free energy values corroborate that **2a** is the most-stable isomer by 5.1 or 5.9 kcal·mol^{-1} depending on the phase, gas or solvent, respectively (Figure 4). Those results corroborate the experimental finding that **2a** is the kinetically favored isomer whereas **2b** is the thermodynamically preferred one.

All possible geometrical isomers of the complex [$RuCl_2$-(bpea)(DMSO-S)] with the bpea ligand acting in either meridional or facial fashion were also computed. In the meridional case, the *cis,mer*-dichloro complexes **2a′** (with the DMSO ligand at the opposite side as the ethyl group of bpea, Figure 4) and **2a″** (with the DMSO group in the same side of *N*-ethyl bpea) were found to be at 0.3 and 4.6 kcal·mol^{-1} higher in Gibbs free energy (solvent effects included) than in the *trans,mer*-dichloro **2a** (Figure 4). For the facial case, only the *trans,fac*-dichloro **2b′** isomer is possible, where the DMSO ligand is trans to the aliphatic nitrogen atom of bpea, and is 1.8 kcal·mol^{-1} above the Gibbs free energy of the isolated *cis,fac* **2b**.

For the isomerization of **2a** into **2b**, we have envisaged two different mechanistic scenarios, one that does not involve any bond breaking and that is termed "intramolecular rearrangement mechanism" (*im*, Figure 5) and a second one that involves the breaking and formation of a Ru−Cl bond that will be termed "dissociative mechanism" (*dm*, Figure 6). The intramolecular rearrangement mechanism has been studied by a linear transit in which the N3−Ru−N2−N1 dihedral angle changes from 180 to 90° while the rest of the internal coordinates are fully optimized. The energy profile obtained in this way does not represent the intrinsic reaction path but rather sets an upper limit for the activation barrier of the process. Certainly this linear transit is not optimal, but it contains the essential features of the intrinsic reaction paths and ensures that the approximate transition state found connects the reactant and the product for the rearrangement under investigation. The energy profile obtained in this way presents a maximum at 140°, with an upper-bound energy

(36) (a) Basallote, M. G.; Durán, J.; Fernández-Trujillo, M. J.; Máñez, A. *J. Chem. Soc., Dalton Trans.* **1998**, 3227−3231. (b) Noda, K.; Ohuchi, Y.; Hashimoto, A.; Fujiki, M.; Itoh, S.; Iwatsuki, S.; Noda, T.; Suzuki, T.; Kashiwabara, K.; Takagi, H. D. *Inorg. Chem.* **2006**, *45*, 1349−1355. (c) Gamasa, M. P.; Gimeno, J.; González-Bernardo, C.; Martín-Vaca, B. M. *Organometallics* **1996**, *15*, 302−308.

(37) (a) Davies, J. A. *Adv. Inorg. Chem. Radiochem.* **1981**, *24*, 115−187. (b) Coe, B. J.; Glenwright, S. J. *Coord. Chem. Rev.* **2000**, *203*, 5−80.

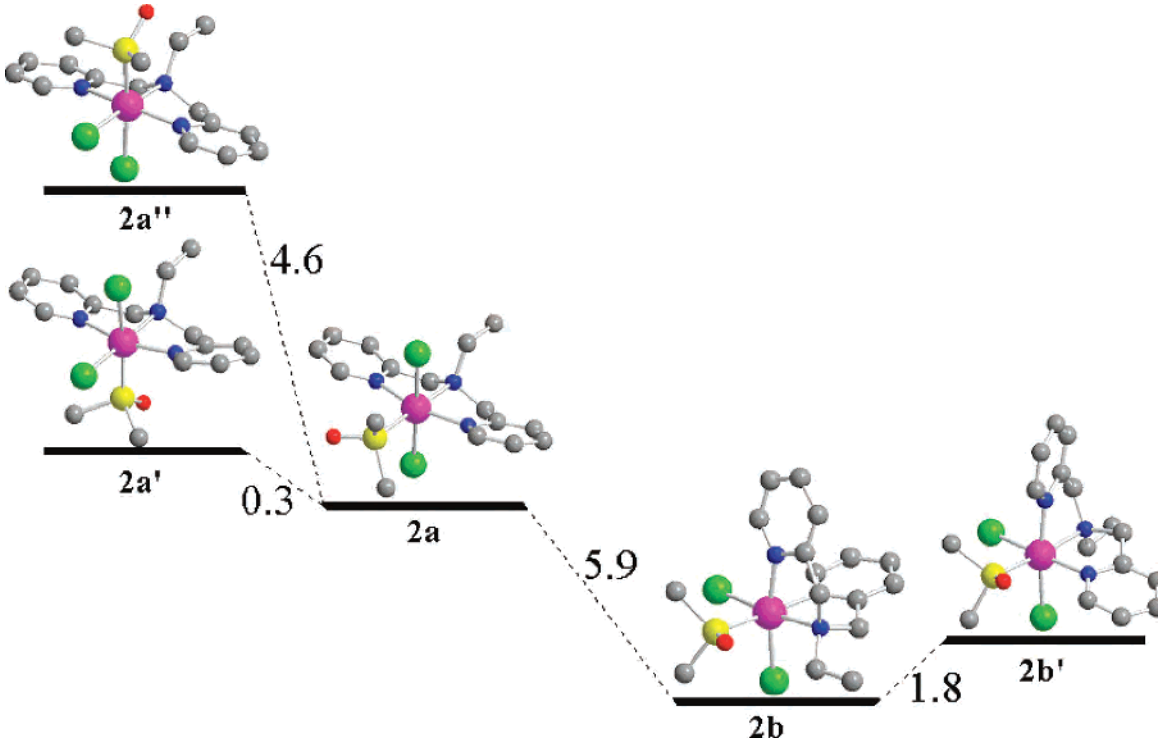

Figure 4. Energy diagram for isomers **2a**, **2a′**, **2a″**, **2b**, and **2b′** including solvent effects (Gibbs free energies in kcal·mol^{-1}).

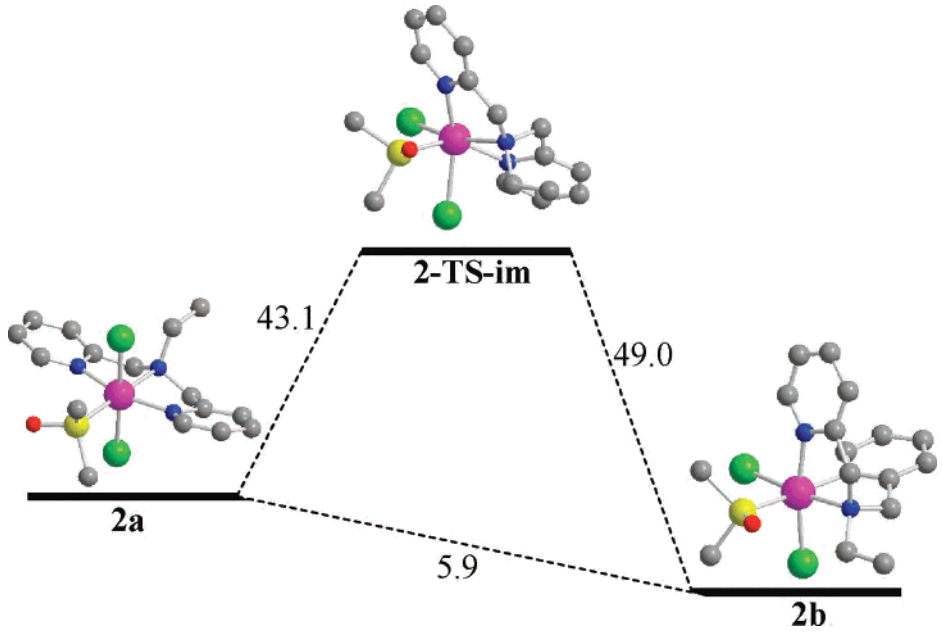

Figure 5. Energy diagram of the intramolecular isomerization mechanism including solvent effects (Gibbs free energies in kcal·mol^{-1}).

barrier of 43.1 kcal·mol^{-1}. The approximate transition state structure, **2-TS-im**, as well as the energy diagram are presented in Figure 5. Solvent effects have a negligible influence on the energetics of this mechanism, given the neutral nature of all of the species involved and the fact that the ruthenium metal center is always hexacoordinated. For the dissociative mechanism, we have assumed the breaking of a Ru−Cl bond as suggested by the kinetic analysis described above, followed by ligand reorganization including the facial to meridional conformation for the bpea ligand, and finally Ru−Cl bond formation as depicted in Figure 6. In contrast to the previous case, here solvent effects are very important because of the charged nature of all of the reaction intermediates and transition states. The first-step Ru−Cl bond dissociation requires 16.8 kcal·mol^{-1}, whereas the second process reorganization to reach the pentacoordinated **2-TS-dm** is 9.2 kcal·mol^{-1}, both including solvent effects. The rather-low energy value for the heterolytic Ru−Cl cleavage is not unexpected,[38] and it is a consequence of the high solvation energy of the chloride anion in polar solvents.

Overall, the Gibbs free energy barrier through this mechanism is 26.0 kcal·mol^{-1} and is thus theoretically favored

(38) Rossin, A.; Gonsalvi, L.; Phillips, A. D.; Maresca, O.; Lledós, A.; Peruzzini, M. *Organometallics* **2007**, *26*, 3289−3296.

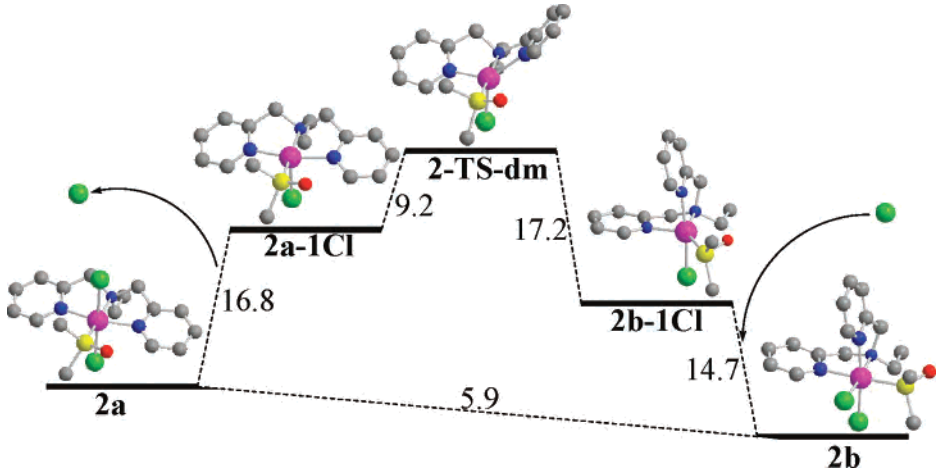

Figure 6. Dissociative mechanism involving chloro elimination including solvent effects (Gibbs free energies in kcal·mol^{-1}).

with regard to the intramolecular rearrangement, in excellent agreement with the kinetic experiments just described.

Furthermore, activation entropies are also in agreement with a dissociative mechanism being the rate-determining step. Theoretically, the intramolecular process presents a negative entropy value of −5.9 cal·mol^{-1}·K^{-1}, whereas the dissociative process presents a clearly positive entropy of 29.2 cal·mol^{-1}·K^{-1}.

Conclusions

As expected, the intrinsic properties of the bpea ligand such as its flexibility, geometry, and the combination of aliphatic and aromatic nitrogen donor atoms confers a combination of properties in octahedral ruthenium complexes, allowing the preparation of a family of related complexes with specific reactivities. In the present work, we have shown that the formation and reactivities follow a complex pattern. Kinetic analysis and DFT calculations have further allowed us to get a deeper insight into the complex reactivity, mechanisms, and structure of intermediates and transition states as well as to elucidate the structure of other isomers that have been neither obtained nor detected. All of the evidence obtained in this article agree that the kinetically favored isomer **2a** does not undergo any thermal reaction substitution up to 80 °C, in sharp contrast with the thermodynamically favored isomer **2b** that can easily exchange either chloro or DMSO ligands. Furthermore, it is also interesting to note that the main reactivity of the **2a** isomer is its interconversion/isomerization to the stable but substitutionally labile **2b** isomer.

Acknowledgment. This research has been financed by MEC of Spain through projects CSD2006-003, CTQ2006-15634, CTQ2005-08797-C02-01, CTQ2006-01080, CTQ2007-60476/PPQ, and CTQ2007-67918. J.M. and A.P. are grateful for the allocation of doctoral grants of the Generalitat de Catalunya and MEC, respectively. A.L. and I.R. also thank Johnson and Matthey for a $RuCl_3 \cdot xH_2O$ loan.

Supporting Information Available: Additional spectroscopic (UV−vis, NMR, ESI) and electrochemical data related to **2**−**3** together with CIF files. This material is available free of charge via the Internet at http://pubs.acs.org. The supplementary crystallographic data can also be obtained free of charge via the Cambridge Crystallographic Data Centre, 12, Union Road, Cambridge CB2 1EZ, U.K.; fax +44 1223 336033 or by e-mail at deposit@ccdc.cam.ac.uk.

IC701421W